Drug Design, Development and Therapy

Dovepress
open access to scientific and medical research

Open Access Full Text Article

ORIGINAL RESEARCH

Integrated Metabolomics and Network Pharmacology to Reveal the Mechanisms of Gandouling Tablets Against Copper-Overload-Induced Neuronal Injury in Rats with Wilson's Disease

Li Chen[1], Wang-Yang Xu[2], Hao Chen[1], Yan-Quan Han[1], Yu-Ting Zhang[1]

[1]The First Affiliated Hospital, Anhui University of Traditional Chinese Medicine, Hefei, People's Republic of China; [2]The College of Pharmacy, Anhui University of Traditional Chinese Medicine, Hefei, People's Republic of China

Correspondence: Hao Chen; Yanquan Han, The First Affiliated Hospital, Anhui University of Traditional Chinese Medicine, Hefei, People's Republic of China, Email chenhao071522@163.com; hyquan2003@163.com

Purpose: Gandouling Tablets (GDL), a proprietary Chinese medicine, have shown a preventive effect against Wilson's disease (WD)-induced neuronal damage in previous studies. However, the potential mechanisms need additional investigation. Combining metabonomics and network pharmacology revealed the GDL pathway against WD-induced neuronal damage.

Methods: The WD rat model with a high copper load was developed, and nerve damage was assessed. Total metabonomics was used to identify distinct hippocampus metabolites and enriched metabolic pathways in MetaboAnalyst. The GDL's possible targets against WD neuron damage were then determined by network pharmacology. Cytoscape constructed compound metabonomics and pharmacology networks. Moreover, molecular docking and Real-Time Quantitative Polymerase Chain Reaction (RT-qPCR) validated key targets.

Results: GDL reduced WD-induced neuronal injury. Twenty-nine GDL-induced metabolites may protect against WD neuron injury. According to network pharmacology, we identified three essential gene clusters, of which genes in cluster 2 had the most significant impact on the metabolic pathway. A comprehensive investigation identified six crucial targets, including UGT1A1, CYP3A4, CYP2E1, CYP1A2, PIK3CB, and LPL, and their associated core metabolites and processes. Four targets reacted strongly with GDL active components. GDL therapy improved five targets' expression.

Conclusion: This collaborative effort revealed the mechanisms of GDL against WD neuron damage and a way to investigate the potential pharmacological mechanisms of other Traditional Chinese Medicine (TCM).

Keywords: GDL, metabonomics, network pharmacology, mechanisms

Introduction

Wilson's disease (WD) is a copper excretion disorder caused by a copper transporter P-type ATPase gene (ATP7B) mutation. Copper accumulates abundantly in most organs, remarkably the eyes, liver, and brain,[1] during disease progression, resulting in liver, brain, kidney, musculoskeletal and other symptoms. Copper accumulation, which which alters gene expression, mitochondrial function, protein suppression, and oxidative stress, may be the cause[1] The excessive accumulation of copper in astrocytes in the brain breaches the blood-brain barrier, exposing neurons and oligodendrocytes directly to increased copper surroundings and causing damage.[1] In current treatments, copper chelation or intestinal zinc absorption limits excess copper from entering the body.[1] Penicillin (D-penicillamine) is commonly used since it is inexpensive, effective, and helpful in treating liver problems, particularly WD.[2–4] However, its medical application is limited due to numerous side effects, like gastrointestinal reactions, fever, rash, leukopenia, nephritis, and systemic lupus erythematosus.[5]

Received: 15 March 2023
Accepted: 6 June 2023
Published: 13 June 2023

Graphical Abstract

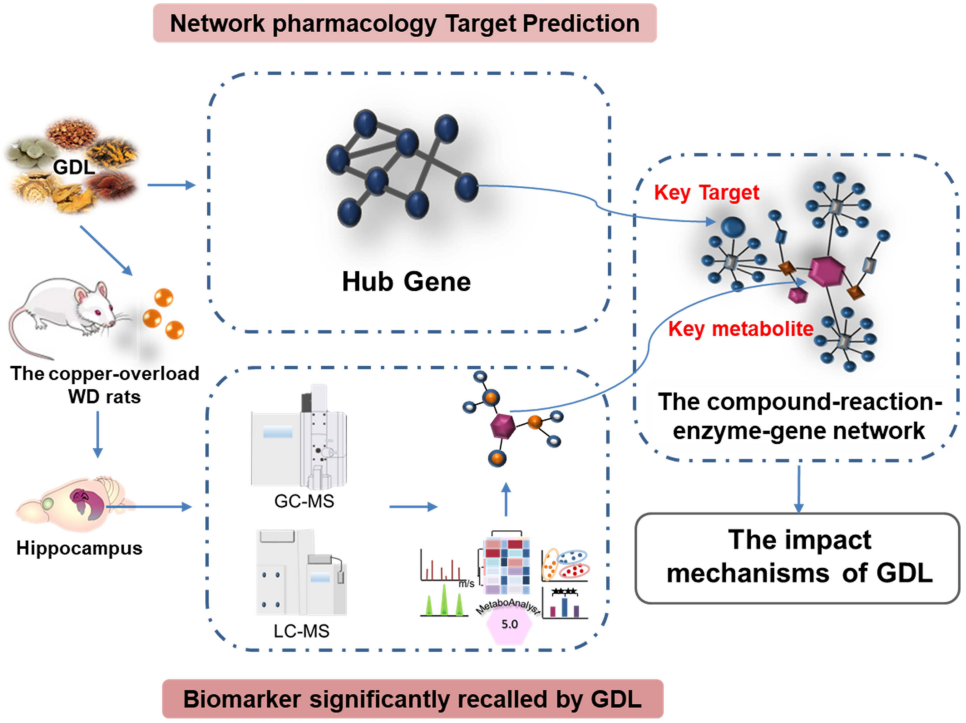

Traditional Chinese Medicine (TCM) balances and treats many complicated disorders with Chinese herbs and herbal formulae.[6] Gandouling Tablets (GDL) are a proprietary Chinese medication validated in China for WD therapy for decades before 2005. (Z20050071). It is based on the long-term clinical experience of Xin'an medical specialist, who stressed the significance of "copper toxicity, moist heat, phlegm, and blood stasis"[7] in WD etiology, formulated the treatment for "clearing heat and poison, reducing blood stasis and softening the hard, and boosting the gallbladder and removing copper"[7] and developed Xin'an characteristic preparations. It fully reflects traditional Chinese medicine's qualities of treating symptoms and underlying causes and "combining syndrome differentiation with illness differentiation and holistic therapy".[7] It consists of six traditional Chinese medicines: *Rheum officinale* Baill. (Dahuang, DH), *Coptis chinensis* Franch. (Huanglian, HL), *Spatholobus suberects* Dunn. (Jixueteng, JXT), *Curcuma longa* L. (Jianghuang, JH), *Salvia miltiorrhiza* Bge. (Danshen, DS), and *Curcuma phaeocaulis* Vai. (Ezhu, EZ) with the weight composition of 1:2:1:1:1:1 (Figure S1) (All the plant names had been checked through MPNS (http://mpns.kew.org)). The GDL preparation procedure was optimized through the use of orthogonal design.[8] HPLC was used to monitor the concentration of GDL's active ingredients for quality control purposes.[9,10] Using ultra-performance liquid chromatography/quadrupole time-of-flight mass spectrometry (UPLC-QTOF/MS), the chemical components and blood components of GDL were identified.[11] Modern clinical data have conclusively proved that it has a substantial role in clearing blood stasis in the liver and gallbladder, removing copper, and improving blood circulation. It is a safe and effective Chinese patent medication.[12–14] Numerous studies have demonstrated that it improves liver function and neuropathy in clinical, animal, and cellular models. Our earlier research has shown that GDL plays a significant neuroprotective impact in WD.[12,15] However, the mechanisms and targets of GDL in treating WD have not been fully elucidated. Thus, it is essential and advantageous to research the putative GDL impact pathway in treatingWD.

Considering the multi-target impact and the characteristics of TCM's systematic regulation, the combined analysis of metabonomics and network pharmacology helps elucidate the likely comprehensive pathways of TCM.[16,17] Metabolomics was used to identify recalled metabolic markers to predict GDL's metabolic regulating mechanism in

copper-overload-induced WD neuronal injury rats. We investigated the genes, metabolic pathways of GDL against WD neuronal injury using network pharmacology. The approach organically integrates external components with metabolic phenotype; the two ways can successfully compensate for each other's deficiencies. Based on experiments, drug binding targets, upstream molecular pathways, and downstream metabolites can define TCM mechanisms. Combining the active components of GDL with metabolic phenotypes helped elucidate the treatment theory of GDL for WD neuronal injury. This study offers a unique perspective on the neuroprotective pathways of GDL in WD patients.

Materials and Methods

Animal Experiments

Reagents

GDL (batch number 20210827) were produced by the First Affiliated Hospital of the Anhui University of TCM. Copper sulphate anhydrous was ordered from China's Fuchen (Tianjin) Chemical Reagent Co., Ltd. (batch number 20211019). High copper feed (1 g $CuSO_4$ / kg) was ordered from Henan Huanyu Hekang Biotechnology Co., Ltd., China. Watson's distilled water was employed. Ethanol, xylene (analytical pure), and paraffin were ordered from Shanghai Suyi Chemical Reagent Co., Ltd., China.

Establishment of Animal Models

Our animal studies were approved by the Animal Ethics Committee of Anhui University of Traditional Chinese Medicine (ID: 2022-039) on 11-21-2022 and conducted in the Animal Experiment Center of Anhui University of TCM by the use and care of Experimental experimental animals' developed by the United States National Institutes of Health and the Prevention of Animal Abuse Act of China (1986). All male Wistar rats (4 months old, 180 ± 20 g, Jinan Pengyue Experimental Animal Breeding Co., Ltd., License No. SCXK 2019-0003) adapted to a 12 h light/dark cycle environment of 22 ± 2 °C and 55 ± 5% humidity for seven days.

The therapeutic impact of GDL on WD was examined using a high copper-loaded rat model in a previous study.[18,19] We experimented according to the method described in the preceding article.[19,20] All rats (n = 23) were divided into model and control groups. In the model group (n = 16), a copper-rich diet caused neuronal damage. The control group received regular feed and distilled water. The model group received 0.185% $CuSO_4$ water and 1 g/kg $CuSO_4$ feed daily. After six weeks, eight rats were randomly assigned to the model group and eight to the GDL group. Copper-rich diets and gavage continued for six weeks. During these six weeks, rats in the GDL group received 2.916 g GDL/kg/d (six times the dose determined based on adult daily intake), while rats in the control and model groups received 10 mL/kg/d of normal saline. The experimental design is depicted in Figure 1A.

Determination of Copper Content

Briefly, 300 mg of carefully weighed cortex sample was placed in a reaction tube, and 6 mL of nitric acid (Guaranteed reagent, Guangzhou Diren Technology Co., Ltd, China) was added. The samples were placed on a heating plate (Heat plater iii, CAMAG Switzerland) at 130 °C for about 30 min to undergo digestion. Then we put them inside the microwave oven for microwave digestion (Multiwave 3000 Microwave Digester, Antonpa, Austria).[21] ICP-MS measured the copper concentration (7800, Agilent, U.S.A.).

Biochemical Detection

We measured alanine aminotransferase (ALT), aspartate aminotransferase (AST), ceruloplasmin (CP), hyaluronic acid (HA), laminin (LN), type IV collagen (COL4), and procollagen III n-terminal propeptide (PIIINP) in peripheral serum before and after drug intervention to evaluate the animal model and drug intervention. The Nanjing Jiancheng Bioengineering Research Institute provided ALT and AST test kits (Nanjing, China). The ELISA kits for CP, HA, LN, COL4, and PIIINP were purchased from Wuhan Genmei Technology Co., Ltd. (Wuhan, China). All the samples were analyzed directly. Each trial was repeated thrice per the kit's instructions.

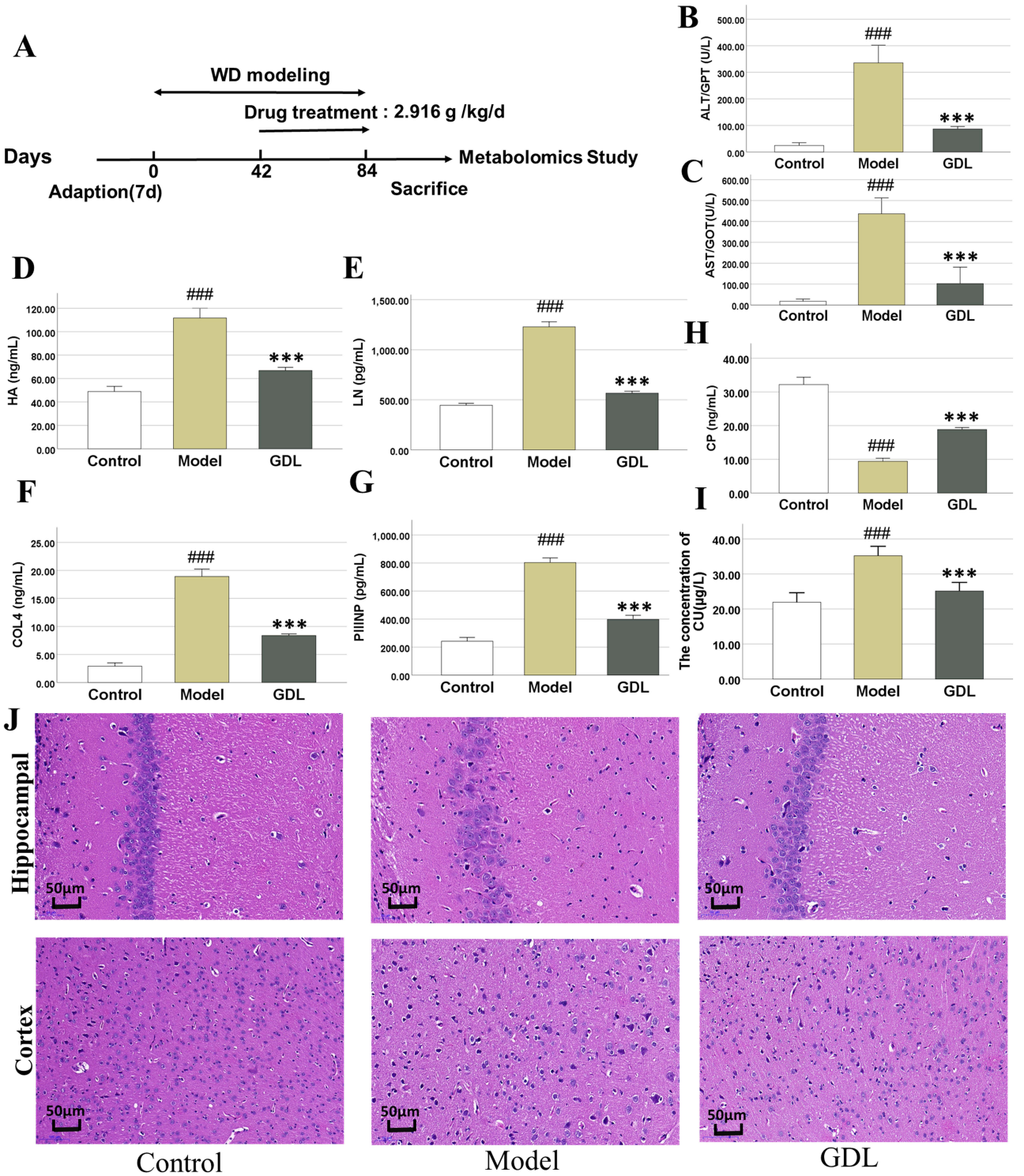

Figure 1 (**A**) WD and drug treatment program schedule schematic diagram. (**B**–**I**) Determination of ALT, AST, CP, HA, LN, COL4, PIIINP, and CU Levels. All data were expressed as mean ± SD (n = 6). ###p < 0.001, compared with the control group; ***p < 0.001, compared with the model group. (**J**) Morphological changes in the hippocampal CA1 area and cerebral cortex of rats in each group (HE staining) (50 μm).

Hematoxylin-Eosin (HE) Staining

Pathological analysis revealed differences in the cortex morphology and CA1 area of the hippocampus. The brain tissue was preserved in a 4% formalin solution for 8 h at 4 °C (AG29787889, HyClone, U.S.A.). Dehydration in low to high alcohol concentrations (70% ethanol solution, 5 min; 80%, 90%, 95%, and absolute ethanol, 4 h each time). Tissues were

immersed in paraffin after 30 min in xylene. In the cross-region (containing the hippocampus), 3 μm coronal slices were made. Each sample had ten HE segments extracted for HE tests.

Metabolomics Analysis

Reagents

Acetonitrile, methanol, and formic acid (chromatography grade) were purchased from Thermo Fisher Scientific Inc. N-Hexane from CNW (Germany). L-2-chlorophenyl alanine and chloroform (analytical pure) were acquired from Shanghai Hengchuang Biotechnology Co., Ltd., China. A fatty acid methyl esters (octanoic (C8:0), azelaic (C9:0), decanoic (C10:0), dodecanoic /lauric (C12:0), tetradecanoic /myristic (C14:0), hexadecanoic /palmitic (C16:0), octadecanoic /stearic (C18:0), eicosanoic /arachidonic (C20:0), docosanic /shanshu (C22:0), and Methyl pentadecanoate/methyl xylate (C24:0)) was purchased from Nu-chek, Dr.Ehrenstorfer. The chromatography-grade water was acquired from the Wahaha Group.

Samples for LC-MS Analysis

Typically, 30 mg of hippocampus sample was weighed precisely, and two small steel balls were put in a 1.5 mL Eppendorf tube. Each sample was frozen at −20 °C for 2 min after being supplemented with 20 μL L-2-chlorophenyl alanine (0.06 mg/mL) dissolved in methanol as internal standard and 600 μL combination of methanol and water (4/1, vol/vol). Followed by 2 min of grounding at 60 Hertz (full-automatic sample rapid grinder, Wonbio-96E, Shanghai Wanbo Biotechnology Co., Ltd.). Ten min of ultrasonic extraction in an ice bath was followed by 5 h at −20 °C. Specimens were centrifuged at 4 °C for 10 min (13,000 rpm). Supernatant at −80 °C was the sample solution. Quality control (QC) samples were blended from all samples made using the preceding method.

Samples for GC-MS Analysis

In a 1.5 mL Eppendorf tube, a 30 mg hippocampus sample and two small steel balls were placed. Then, 20 μL of an internal standard solution (L-2-chlorophenyl alanine dissolved in methanol, 0.06 mg/mL) and 600 μL of a methanol/water (4/1, vol/vol) solution were added. After 2 min of storage at −80°C ground it at 60 Hz for 2 min (full-automatic sample rapid grinder, Wonbio-96E, Shanghai Wanbo Biotechnology Co., Ltd.). Typically, 120 μL of chloroform was added, swirled in a vortex, ultrasonically extracted in ice water for 10 min, and then frozen at - 20 °C for 30 min. The specimens were centrifuged at 4 °C (13,000 rpm) for 10 min (high-speed freezing centrifuge, TGL-16MS, Shanghai Luxianyi Instrument Co., Ltd.). About 150 μL of supernatant was taken and dried in a centrifugal freezer (LNG-T98, Taicang Huamei Biochemical Instrument Factory). Then 80 μL of a 15 mg/mL pyridine solution of methoxyl amine hydrochloride was added, the mixture was violently agitated for 2 min (vortex oscillator, MX-S, Beijing Dalong Xing Chuang Instrument Co., Ltd.), and it was incubated at 37 °C for 90 min (gas bath thermostatic oscillator, SHZ-82, Shanghai Lichen Instrument Technology Co., Ltd.). Finally added, 50 μL the mixture BSTFA (including 1% TMCS), 20 μL n-hexane, and internal standard (C8:0/C9:0/C10:0/C12:0/C14:0/C16:0/C18:0/C20:0/C22:0/C24:0, both soluble in chloroform, 10 μL for each). The mixture was vortexed rapidly for 2 min and then deviated at 70 °C for 60 min. All samples were prepared as above and blended uniformly to obtain QC samples.

LC-MS Analysis

Using the Dionex Ultimate 3000 RS UHPLC with a heated electric spray ionization (ESI) source (Thermo Fisher Scientific, Waltham, MA, USA) and Q-Exactive quadrupole orbit mass spectrometer, the metabolic spectrum of the samples was measured in ESI positive and ESI negative ion modes. ACQUITY UPLC HSS T3 COLUMN (1.8 m. 2.1100 mm) used for sample separation. The elution solvent is (A) water (mic acid, v/v, containing 0.1%) and (B) acetonitrile (mic acid, v/v), and the elution gradient is 0.01 min, 5% B; 2 min, 5% B; 4 min, 30% B; 8 min, 50% B; 10 min, 80% B; 14 min, 100% B; 15 min, 100% B; 15.1 min, 5% and 16 min, 5% B. Flow rate 0.35 mL/min, column temperature 45°C. 100–1200 m/z mass range. The solution was adjusted to 70,000 for full MS scans and 17,500 for HCD MS/MS scans. The mass spectrometer functioned as follows: The capillary temperature is 320 °C, the spray voltage is 3800 volts (+) and 3000 volts (−), the sheath gas flow rate is 40 arbitrary units (+) and 35 arbitrary units (−), and the auxiliary gas flow rate is 10 arbitrary units (+) and 8 arbitrary units (−).

GC-MS Analysis

The derivative specimens were analyzed using Agilent 7890B gas chromatography and Agilent 5977B MSD systems (Agilent Technologies Inc., CA, USA). DB-5MS fused-silica capillary column (30 m × 0.25 mm × 0.25 μm, Agilent J&W Scientific, Folsom, CA, USA) was used as the chromatographic column to distinguish the derivatives. The steady flow rate of the carrier gas (Helium, > 99.999%) across the column was 1 mL/min. The injector temperature was kept constant at 260 °C. Briefly, 1 μL was the injection volume in splitless mode. The initial temperature of the oven was 60 °C, which was held for 0.5 min before being increased to 125, 210, 270, and 305 °C at rates of 8, 8, 15, and 20 °C/min, respectively, and then held at 305 °C for 5 min. The MS quadrupole and ion source (electron impact) temperatures were fixed at 150 and 230 °C, respectively. Mass spectrum data (m/z, 50–500) was collected using the full scan mode.

Data Preprocessing and Statistical Analysis

Gas-chromatography- mass spectrometry (GC-MS) and liquid chromatography-mass spectrometry (LC-MS) raw data were loaded into the programs MS-DIAL and Progenesis QI V2.3 (Nonlinear, Dynamics, Newcastle, UK), respectively. For qualitative analysis, GC-MS Metabolite characteristics depended on the LUG database (The untargeted database of GC-MS from Luming Bio). LC-MS were dependent on the isotopic distribution, secondary fragments, and specific mass-to-charge ratio (M/z) using the PMDB, EMDB, Lipidmaps (V2.3), Metlin (Untargeted database of LC-MS from Luming bio), and Human Metabolome Database (HMDB). After screening to get the GC/MS and LC-MS data matrix, all peak signal intensities of the specimens were separated and normalized based on the features of QC samples with a relative standard deviation (RSD) greater than 0.3. Principal Component Analysis (PCA) was used to examine specimen distribution and analytical technique stability by importing the LC-MS and GC/MS matrix into R. Group differences were assessed using Partial Least Squares Discriminant Analysis (PLS-DA) and Orthogonal Partial Least Squares Discriminant Analysis (OPLS-DA). 7-fold cross-validation and 200 response permutation tests (RPT) were used to measure model quality. Using a two-tailed Student's *t*-test, it was determined whether the differences in metabolites between the groups were statistically significant. Metabolites with Variable Importance of Projection (VIP) values of more than 1.0 and p-values less than 0.05 were chosen. The pheatmap R package was utilized to display heat maps. To investigate metabolic mechanics, MetaboAnalyst 5.0 (https://www.metaboanalyst.ca) was employed.

Network Pharmacology Analysis

To identify essential metabolites and associated proteins, we built an optical compound-reaction-enzyme-gene network using Cytoscape 3.9.0 (Cytoscape Consortium, CA, USA). Four steps were involved. (1) The target prediction of GDL against WD nerve injury. The targets of neuron damage caused by WD were screened in Online Mendelian Inheritance in Man (OMIM, https://omim.org/) and Genecards (https://www.genecards.org/). Encyclopedia of Traditional Chinese Medicine (ETCM, http://www.nrc.ac.cn:9090/ETCM/), bioinformatics analysis tools (BATMAN-TCM, http://bionet.ncpsb.org/batman-tcm/), and TCM systematic pharmacology database and analysis platform (TCMSP, http://lsp.nwu.edu.cn/tcmsp.php) were employed to obtain GDL molecular targets. Their intersection was the prediction target of GDL against WD neuron damage. (2) Using STRING 11.0 to develop protein-protein interaction (PPI) network (https://string-db.org/). The core targets were obtained by using Cytoscape 3.9.0, according to "Degree, betweenness centrality (BC), Closeness centrality (CC), and Local average connectivity (LAC) ≥ Median". The most important modules in the PPI network were defined utilizing Molecular Complex detection (MCODE). (3) The pathway and Gene Ontology (GO) enrichments of potential targets were analyzed by Cytoscape clue GO. KEGG pathway analysis was set to $p < 0.05$. (4) The recalled metabolites identified in metabonomics and the predicted hub targets were integrated into Cytoscape with MetScape to obtain compound-reaction-enzyme-gene and detect important metabolites and proteins. After being reviewed by the Medical ethics committee of the first affiliated hospital of Anhui University of Chinese Medicine (Anhui provincial Hospital of Chinese Medicine), this study's part is based on a study involving publicly available data exempted from ethical review.

Result Validation

Molecular Docking

Traditional Chinese Medicine Systems Pharmacology Database and Analysis Platform (TCMSP, http://lsp.nwu.edu.cn/tcmsp.php) and PubChem Compound (https://www.ncbi.nlm.nih.gov/pccompound, PubChem CID:6443665) were used to obtain the 3D construction of GDL active components related to crucial targets in network pharmacology research. Target structures acquired from the RCSB protein database (https://www.rcsb.org/). Analyses were conducted on cytochrome P-450 (CYP1A2, PDB ID: 2HI4), cytochrome P-45 (CYP2E1, PDB ID: 3E6I), cytochrome P-50 (CYP3A4, PDB ID: 4D7D), and lipoprotein kinase (LPL, PDB ID: 6 OAU). After optimizing by eliminating water molecules and adding hydrogen atoms, we used AutoDockTools 1.5.6 to convert active components and targets from raw to pdbqt. Then, Autodock Vina was employed for molecular docking research. The genetic algorithm was calculated, and the software's default value was executed during docking. PyMoL showed the lowest binding energy docking results.

Real-Time Quantitative Polymerase Chain Reaction (RT-PCR) Analysis

Total RNA was isolated from tissue samples of the right hippocampus using Trizol (Life Technologies, China, 420810). The total RNA concentration and purity were evaluated using ultramicro spectrophotometry (Wuyi, Nanjing, China). The first strand cDNA is generated using a first-strand cDNA synthesis kit following the manufacturer's protocol (AM62082A, TaKaRa, Beijing, China). Real-time PCR detects quantitative RT-PCR (PIKOREAL 96, Thermo Scientific, USA). Based on β- Reference expression of actin, the $2^{-\Delta\Delta Ct}$ method was used for the relative expression level of each gene. The primer sequences used for PCR were as follows: UGT1A1 forward primer: 5′-AATGACTGCCATCTGTTGGT -3', UGT1A1 reverse primer: 5′-AACATGAGCACAGTGAGGAA -3', CYP2E1 forward primer: 5′- AAAAACACAGCCAAGAACCC -3', CYP2E1 reverse primer: 5′- AGGATCAGGAGCCCATATCT -3', CYP1A2 forward primer:5′- CCTCTTCTTAGCCATCCTCC -3', CYP1A2 reverse primer: 5′- ATCTTCACTTGGAGAAGCGT -3', PIK3CB forward primer: 5′- CAGTGCGAACGTATCAAGTC -3', PIK3CB reverse primer: 5′- AATTTTCTCGGCAGTCTTGC -3', LPL forward primer: 5′- TTCCAGCAGCAAAGCAGAA -3', LPL reverse primer: 5′- GTGTCTTCAGGGGTCCTTAG -3', beta-Actin forward primer: 5′- CCCATCTATGAGGGTTACGC -3', beta-Actin reverse primer: 5′- TTTAATGTCACGCACGATTTC -3'.

Statistical Analysis

The outcomes were provided as the mean ± Standard Deviation (SD) of each experimental group's measured results. Single-factor analysis of variance (ANOVA) was used to assess the results, and SPSS 20.0 was used to compare groups using the Student's *t*-test. $p< 0.05$ signified statistical significance.

Results and Discussion

Protective Impact of GDL on the Copper-Overload-Induced Neuronal Damage in Rats with WD

CP affects copper metabolism and is a key WD diagnostic marker.[1] WD develops mostly in the liver and neurological system.[1] We examined the CP levers and its damage states to validate the WD model.

ALT, AST, HA, LN, COL4, and PIIINP levels in the model group were considerably higher than in the control group, although CP levels were significantly lower. The GDL group had lower ALT, AST, HA, LN, COL4, and PIIINP levels than the model group but greater CP. The specifics are illustrated in Figure 1B–H. The fact that the CP level was lower in the model group suggests that copper metabolism was impaired. Other results indicated that copper-treated SD rats had impaired liver function.

The model group's hippocampus Cu concentration was considerably higher than the control group's. The GDL group contained much less Cu than the model group. Details are illustrated in Figure 1I. HE staining revealed structural changes in the CA1 region of the rat hippocampus and cerebral cortex. Figure 1I demonstrated typical micrographs of the cerebral cortex and hippocampus CA1 area. The control group's CA1 hippocampal neurons were compact. The cytoplasm is equally pigmented, like cerebral cortex neurons. The model group had disordered hippocampal CA1 region cells and atrophied cerebral cortex and hippocampus CA1 neurons. In the GDL group, neurons in the CA1 region of the

hippocampus and cerebral cortex resembled those of the control group, and their number was greater than the model group (Figure 1J). The model group's brains had excessive copper levels and damaged hippocampus and cortex.

The results demonstrated that copper-loaded SD rats are accurate and dependable as animal models for studying WD neuronal injury. GDL at the level used in this work had a favorable effect on copper-overload-induced neuronal damage in WD rats.

Results of Metabolomics Analysis

Metabolomics Profiling

LC-MS identified 6069 metabolites, and GC-MS identified 245 metabolites. QC samples assessed metabonomics stability and reproducibility. Figure S2A and B shows that the RSD% of 100 and 94.4% metabolites were < 30% using LC-MS and QC. Moreover, unsupervised PCA (Figure S2C and D) and representative total ion chromatography (TIC) (Figure S2E and F) revealed that QC samples were stable throughout the procedure. These results demonstrate the instrument's high stability and the reproducibility of LC-MS and QC-MS techniques, respectively.

Figure S3A and B display the sample's TIC. Figure 2A shows that specimens from the identical group are collected, but the samples from the control, model, and GDL groups are substantially distinct. According to LC-MS, the R2X, R2Y, and Q2 in PLS-DA were 0.564, 0.881, and 0.666 values, but QC-MS determined the values to be 0.505, 0.894, and 0.673. These results indicated that the model and GDL groups substantially affected metabolic processes.

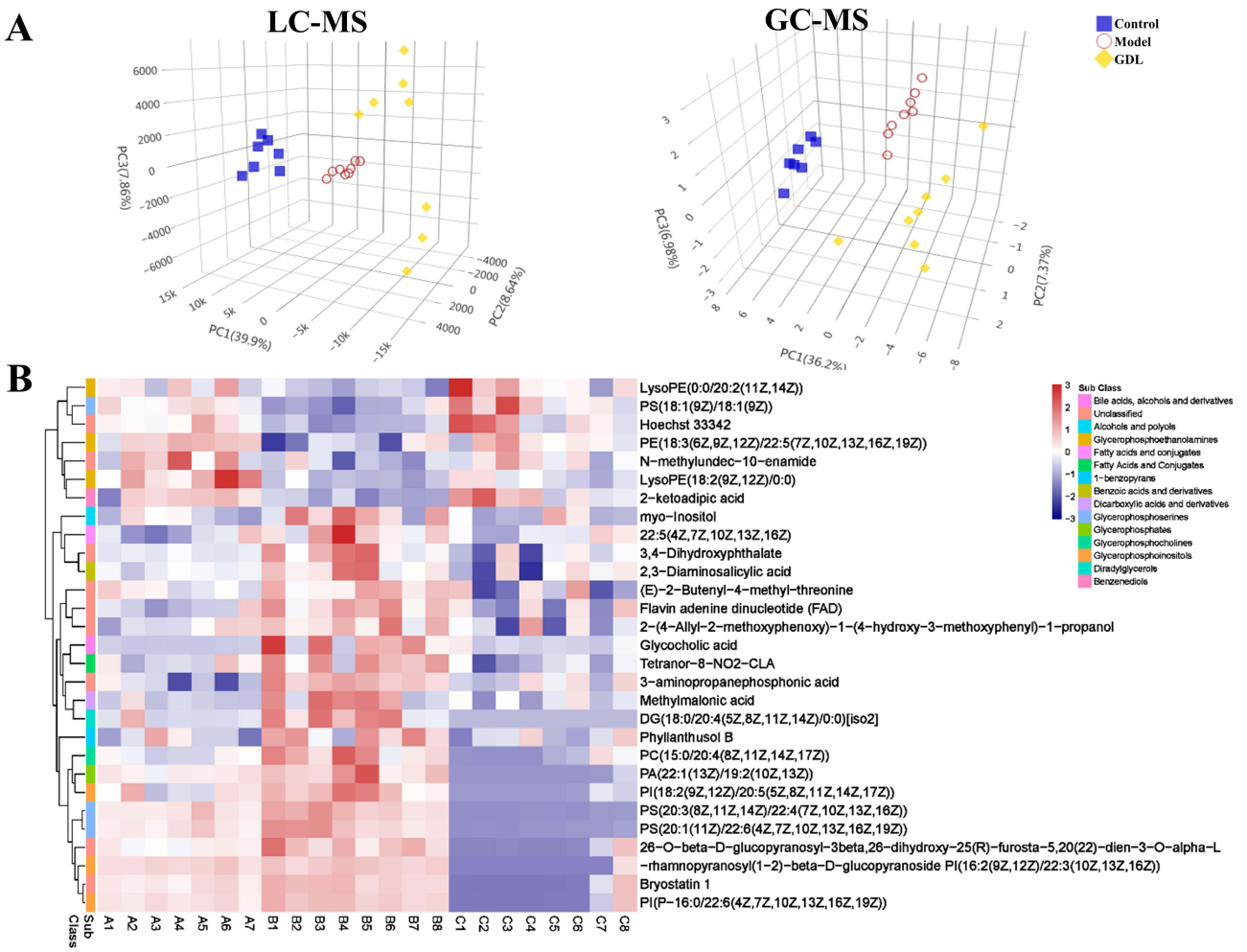

Figure 2 (**A**) PLS-DA score plots of three groups by LC-MS and LC-MS. (**B**) Hierarchical clustering analysis heatmap of differential metabolites in copper-laden WD rats treated by GDL. Red and blue represent that the levels of differential metabolites are higher and lower compared to the average level, respectively.

Recalled Metabolite Identification and Mechanism Analysis

OPLS-DA, student T, and FDR testing showed differential metabolites. Each OPLS-DA model demonstrates significant differentiation, and R2Y and Q2 are high, indicating that the predictive power of cross-validation and the interpretation of sample classification information is excellent (Table S1). Furthermore, 7-fold cross-validation and response alignment tests demonstrated that the model was not overfitted and was trustworthy (Figure S4A–D, Table S1).

Using LC-MS and QC-MS, we found 399 and 97 metabolite markers between the control and the model groups, respectively, depending on VIP>1 and p<0.05. GDL reversed 168 and 23 metabolites (File Table S2). 27 and 2 metabolites altered significantly. The information about these metabolites is included in Table 1 and Table 2.

The typical MS/MS spectrum of the significantly reversed metabolite is shown in Figure S5. We determined the accuracy of metabolites using a multivariate receiver operating characteristic (ROC) curve and predictive accuracy plots (Figure S6A–H). The ROC curve and prediction accuracy chart demonstrated that the diagnostic accuracy of all three patient groups was high.

We developed a heat map to demonstrate the differences in metabolite levels across the three groups. As depicted in Figure 2B, all metabolites were altered in the model group and reversed in the GDL group, suggesting that GDL therapy can reduce metabolic disturbance.

Table 1 The Recalled Metabolites in GDL Treated the Copper-Laden WD Rats by LC-MS

NO.	Ion mode	Metabolites	Formula	VIP (Model/ Control)	P-value (Model/ Control)	P-value (GDL/ Model)
1	Pos	Glycocholic acid	C26H43NO6	1.186	0.007	0.015
2	Pos	Flavin adenine dinucleotide (FAD)	C27H33N9O15P2	2.004	0.001	0.010
3	Neg	Myo-Inositol	C6H12O6	3.818	0.028	0.033
4	Pos	LysoPE(18:2(9Z,12Z)/0:0)	C23H44NO7P	3.442	0.000	0.037
5	Neg	22:5(4Z,7Z,10Z,13Z,16Z)	C22H34O2	4.864	0.020	0.048
6	Pos	LysoPE(0:0/20:2(11Z,14Z))	C25H48NO7P	1.076	0.022	0.018
7	Pos	(E)-2-Butenyl-4-methyl-threonine	C9H17NO3	3.394	0.024	0.035
8	Pos	2-(4-Allyl-2-methoxyphenoxy)-1-(4-hydroxy-3-methoxyphenyl)-1-propanol	C20H24O5	1.432	0.031	0.026
9	Neg	Tetranor-8-NO2-CLA	C14H23NO4	2.018	0.018	0.001
10	Neg	N-methylundec-10-enamide	C12H23NO	1.109	0.023	0.046
11	Neg	Phyllanthusol B	C35H49NO18	1.174	0.036	0.020
12	Pos	3,4-Dihydroxyphthalate	C8H6O6	1.268	0.015	0.012
13	Pos	2,3-Diaminosalicylic acid	C7H8N2O3	1.309	0.021	0.038
14	Pos	Methylmalonic acid	C4H6O4	1.402	0.016	0.022
15	Neg	PS(18:1(9Z)/18:1(9Z))	C42H78NO10P	6.642	0.001	0.003
16	Pos	PA(22:1(13Z)/19:2(10Z,13Z))	C44H81O8P	1.477	0.032	0.000
17	Pos	PC(15:0/20:4(8Z,11Z,14Z,17Z))	C43H78NO8P	2.445	0.005	0.000
18	Neg	PE(18:3(6Z,9Z,12Z)/22:5(7Z,10Z,13Z,16Z,19Z))	C45H74NO8P	2.114	0.006	0.033
19	Neg	Hoechst 33342	C27H28N6O	1.894	0.000	0.009
20	Pos	26-O-beta-D-glucopyranosyl-3beta,26-dihydroxy-25(R)-furosta-5,20(22)-dien-3-O-alpha-L-rhamnopyranosyl(1-2)-beta-D-glucopyranoside	C46H76O17	1.136	0.005	0.000
21	Pos	PS(20:3(8Z,11Z,14Z)/22:4(7Z,10Z,13Z,16Z))	C48H80NO10P	4.513	0.015	0.000
22	Pos	PI(16:2(9Z,12Z)/22:3(10Z,13Z,16Z))	C47H81O13P	1.726	0.044	0.000
23	Pos	PI(18:2(9Z,12Z)/20:5(5Z,8Z,11Z,14Z,17Z))	C47H77O13P	1.706	0.021	0.000
24	Pos	PS(20:1(11Z)/22:6(4Z,7Z,10Z,13Z,16Z,19Z))	C48H80NO10P	5.069	0.028	0.000
25	Pos	DG(18:0/20:4(5Z,8Z,11Z,14Z)/0:0)[iso2]	C41H72O5	1.777	0.010	0.002
26	Pos	Bryostatin 1	C47H68O17	5.702	0.002	0.000
27	Pos	PI(P-16:0/22:6(4Z,7Z,10Z,13Z,16Z,19Z))	C47H79O12P	8.208	0.001	0.000

Table 2 The Recalled Metabolites in GDL Treated the Copper-Laden WD Rats by GC-MS

NO.	Metabolites	Formula	VIP (Model/Control)	P-value (Model/Control)	P-value (GDL/Model)
1	2-ketoadipic acid	C6H8O5	1.296	0.006	0.003
2	3-aminopropanephosphonic acid	C12H34NO3PSi3	1.412	0.001	0.001

The reverse metabolite was added to MetaboAnalyst 5.0 to determine model rat GDL metabolism. As demonstrated in Figure 3 and Table S3, 28 mechanisms in the hippocampus are considerably altered based on $p<0.05$, including the metabolism of aspartic acid, phenylacetic acid, aspartic acid, and purine.

The results showed that GDL strongly regulated metabolites by aspartic acid, phenylacetic acid, and purine metabolic pathways, healing nerve damage in copper-overload-induced rats.

Results of Network Pharmacology Analysis

The Combination Interaction of Compounds and Targets

Based on the TCMSP, ETCM, and TCMSP databases, 299 active complexes and 1715 prospective targets for GDL were identified. From the OMIM and Genecards databases, 657 neuronal targets of WD damage were chosen. Two hundred-eight intersections were evaluated as prospective candidate targets for GDL against neuronal damage caused by WD (Figure S7, Table S4).

PPI Network Construction and Key Targets Screening

Set confidence to medium (0.7) and inspect protein-protein interactions (PPI) with all predicted target genes in the STRING database. The outcome comprised 201 nodes and 1014 edges (Figure S8). Using Median in Cytoscape 3.9.0, the hub targets were screened. The filtering criterion was degree ≥ 7, BC ≥ 84.52114, CC ≥ 0.353982, and LAC ≥ 2.5, yielding 63 nodes and 453 edges (Table S5, Figure 4A). Analysis of the MCODE network revealed 10 clusters (Table S6). Figure 4B illustrates the top three clusters. These important proteins are crucial in the PPI network. The top five hub genes among the 63 hub targets were as follows: SRC (degree 48, Cluster 3), TNF (degree 47, Cluster 1), TP53 (degree 46, Cluster 3), INS (degree 44, Cluster 1), and IL6 (degree 43, Cluster 1).

Analysis of GO Function and KEGG Pathway Enrichment

To predict GDL treatment for WD nerve injury, we used ClueGO to examine the enrichment of GO and KEGG pathways in the first three gene clusters to explain the key targets' neuroprotective effect and GDL's metabolic regulation mechanism (Figure 5A–C). Interestingly, most biological activities in cluster one were characterized as negative regulation of extrinsic apoptotic signaling pathway (37.93%), regulation of epithelial cell apoptotic processing

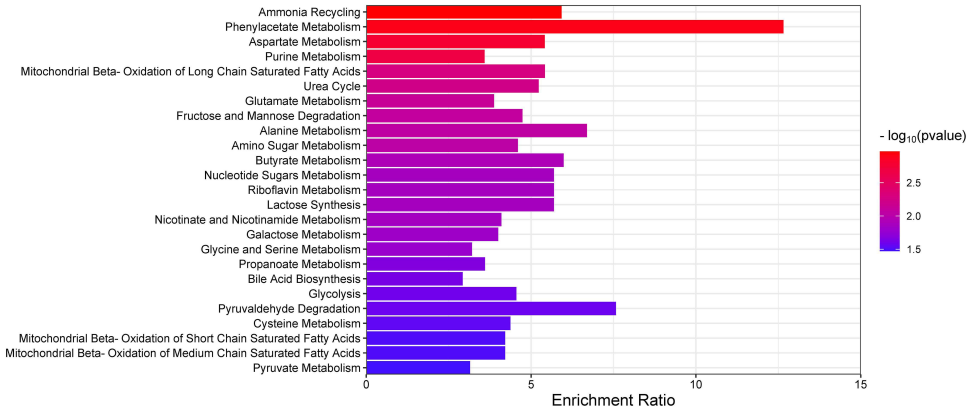

Figure 3 The top 25 metabolic pathways of reversed metabolites in the hippocampus. The red and blue bars reflect the p value. The redder the color, the smaller the p value. The length of the bar represents the enrichment ratio.

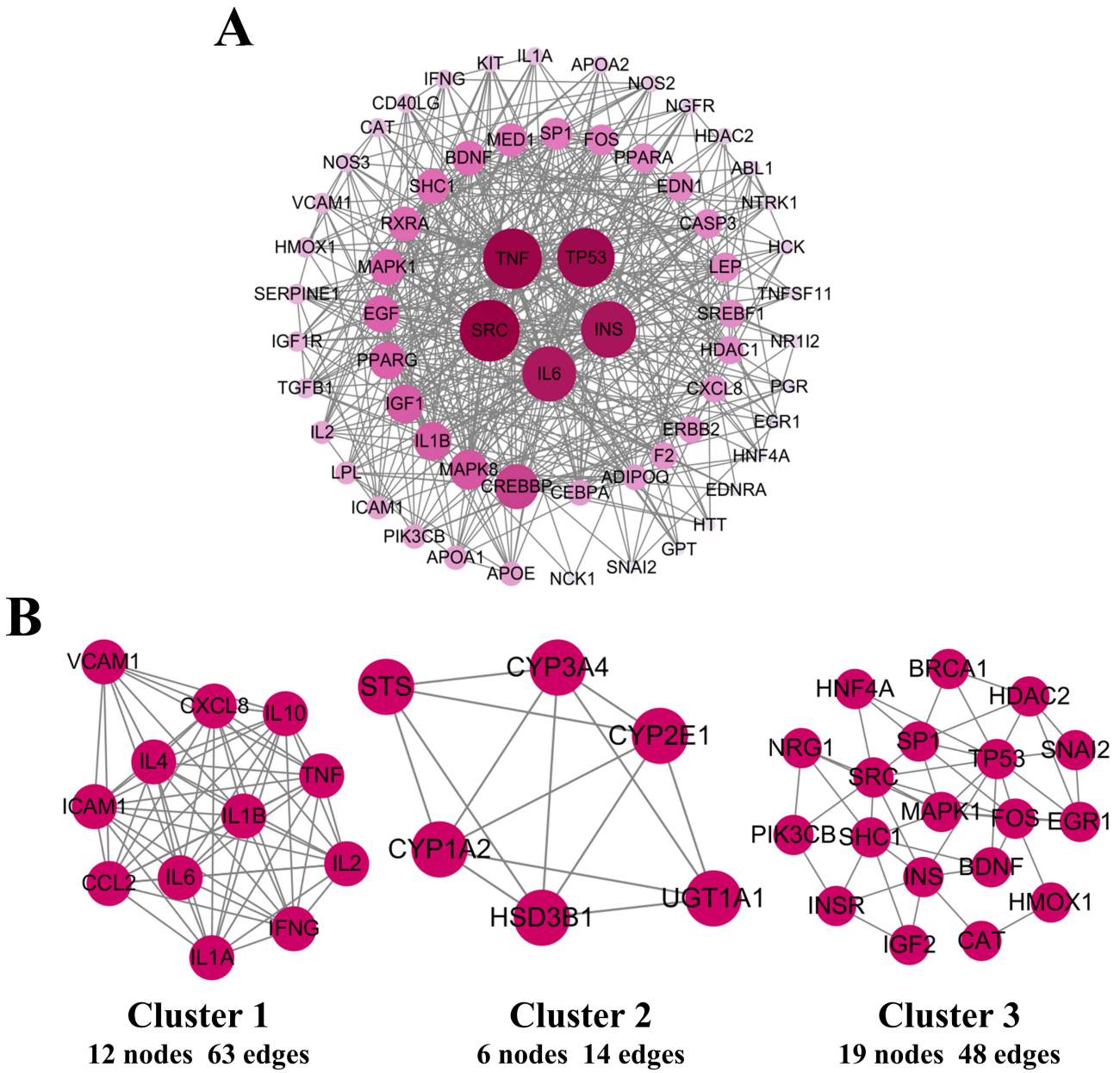

Figure 4 Network construction. (**A**) The hub targets network, which was screened by the median, in which node size reflects its degree, (**B**) The top three clusters analyzed by MCODE network.

(34.48%), and regulation of endothelial cell apoptotic processing (27.59%). These biological activities are of great importance for neuronal damage. Cluster 2 was constructed by monoterpenoid metabolic processing (62.50%), estrogen metabolic processing (25.00%), and steroid catabolic processing (12.50%), which have a significant impact on lipid metabolism. Cluster 3 included insulin-like growth factor receptor binding (57.63%), cellular reaction to hypoxia (16.95%), insulin receptor signaling pathway (11.86%), response to cadmium ion (8.47%), and cellular response to ionizing radiation (5.08%). According to the KEGG enrichment analysis (Figure 6A–C), the metabolic pathways were only enriched in cluster 2 (Figure 6B), with xenobiotics metabolism by cytochrome p450, bile secretion, retinol metabolism, linoleic acid metabolism, and steroid hormone biosynthesis being the metabolic pathways that may be significantly affected.

The results suggested that treating WD nerve damage with GDL involves many components, targets, and metabolic pathways.

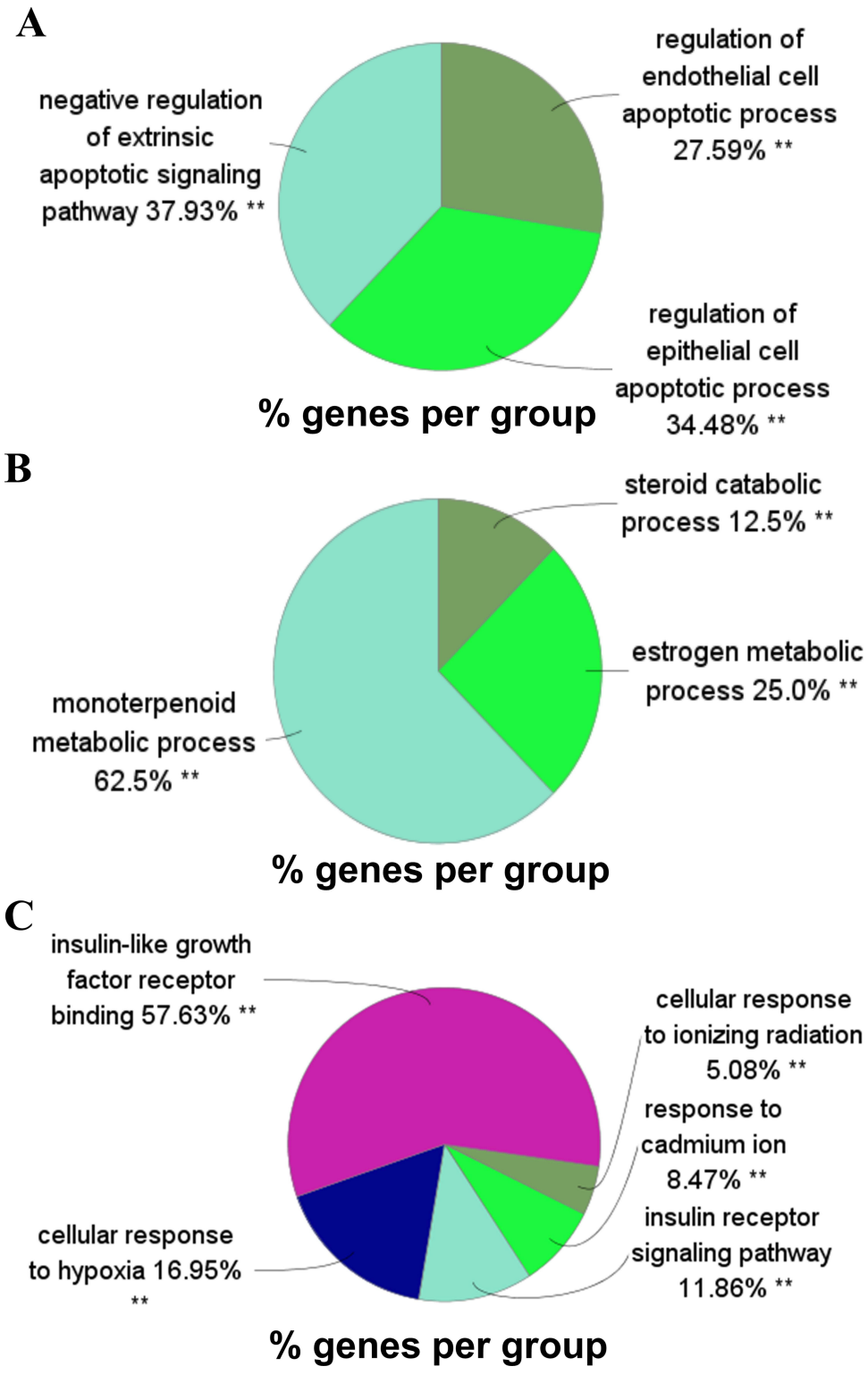

Figure 5 GO enrichment analysis of the top 3 clusters. (**A**–**C**) were the GO terms of clusters 1, 2, and 3 generated by the Cytoscape plug-in ClueGO respectively. The pie chart presented the proportion of each GO terms group. GO, gene ontology. **p < 0.05.

Integrated Analysis of Metabolomics and Network Pharmacology

The metabonomics and network pharmacology interaction network was constructed to examine the mechanisms of GDL against WD neuron damage in depth (Figure 7). Network pharmacology introduces significantly reversed metabolites and possible targets to the Cytoscape MetScape plug-in to build compound-reaction-enzyme-gene networks. We identified six

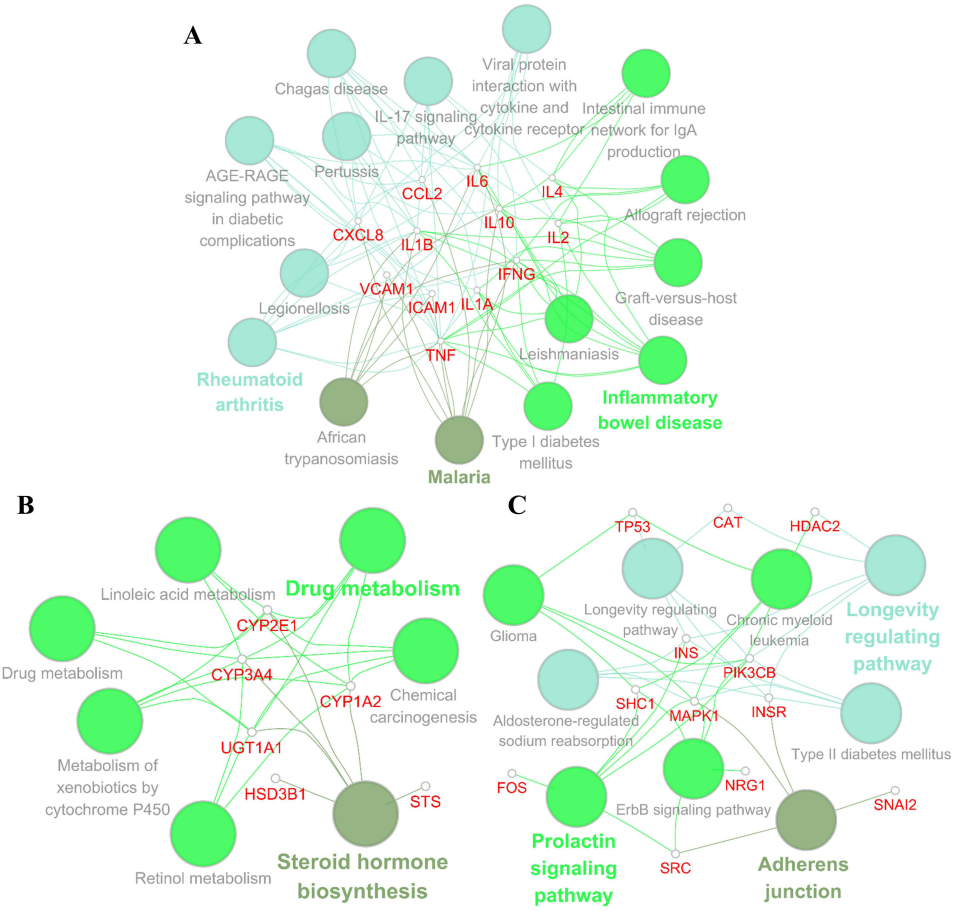

Figure 6 KEGG enrichment analysis of the top 3 clusters. (**A**–**C**) were the interaction network between KEGG terms and genes in clusters 1, 2, and 3 generated by the Cytoscape plug-in ClueGO respectively, in which the effective terms of each group were highlighted. All pathways have a p-value of < 0.05.

crucial network targets, including UGT1A1, CYP3A4, CYP2E1, CYP1A2, PIK3CB, and LPL (Table 3). The related vital metabolites were Phosphatidylethanolamine (PE), Phosphatidylcholine (PC), Diacylglycerol (DC), and Myo-inositol. The impacted mechanisms were Arachidonic acid, Linoleate, Glycerophospholipid, and Phosphatidylinositol phosphate metabolisms. A complex network of interactions was among them, as shown in Figure 7. The metabolic pathways are vital to the therapeutic impact of GDL on WD nerve damage. Among the key targets, UGT1A1, CYP3A4, CYP2E1, and CYP1A2 were hub genes of cluster 2.

Molecular Docking

Using a molecular docking study, we investigated the potential for interaction between important targets and the active GDL components associated with key targets to validate the joint analysis prediction results (File Table S7). The binding free energies are shown in Table S8. Four important targets' 3D structures can be downloaded from the RCSB protein database and studied using molecular docking. Thirteen active molecules of GDL developed hydrogen bond interactions with CYP1A2 at the active site, as determined by docking studies. Three active ingredients were from JH, two from DS, and eight from DH. With a −11.2 kcal/mol, chrysophanol has the lowest binding energy to CYP1A2 among the 13 compounds (Figure 8A). During the interaction with CYP2E1, 10 active GDL compounds formed hydrogen bonds. Eight active components were from DH, while the remaining two came from JXT and EZ. Palmidin C binds to CYP2E1 with the lowest binding energy (−9.6 kcal/mol) (Figure 8B). Eleven active molecules of GDL interacted by hydrogen bonding with CYP3A4. Eight active components were derived from DH, two from DS, and one from HL. Palmidin C and Rheidin C binding energy to CYP3A4 was −10.5 kcal/mol, the lowest of the 11 compounds studied (Figure 8C and D). Three active GDL compounds interacted via hydrogen bonding with LPL. Sitogluside,

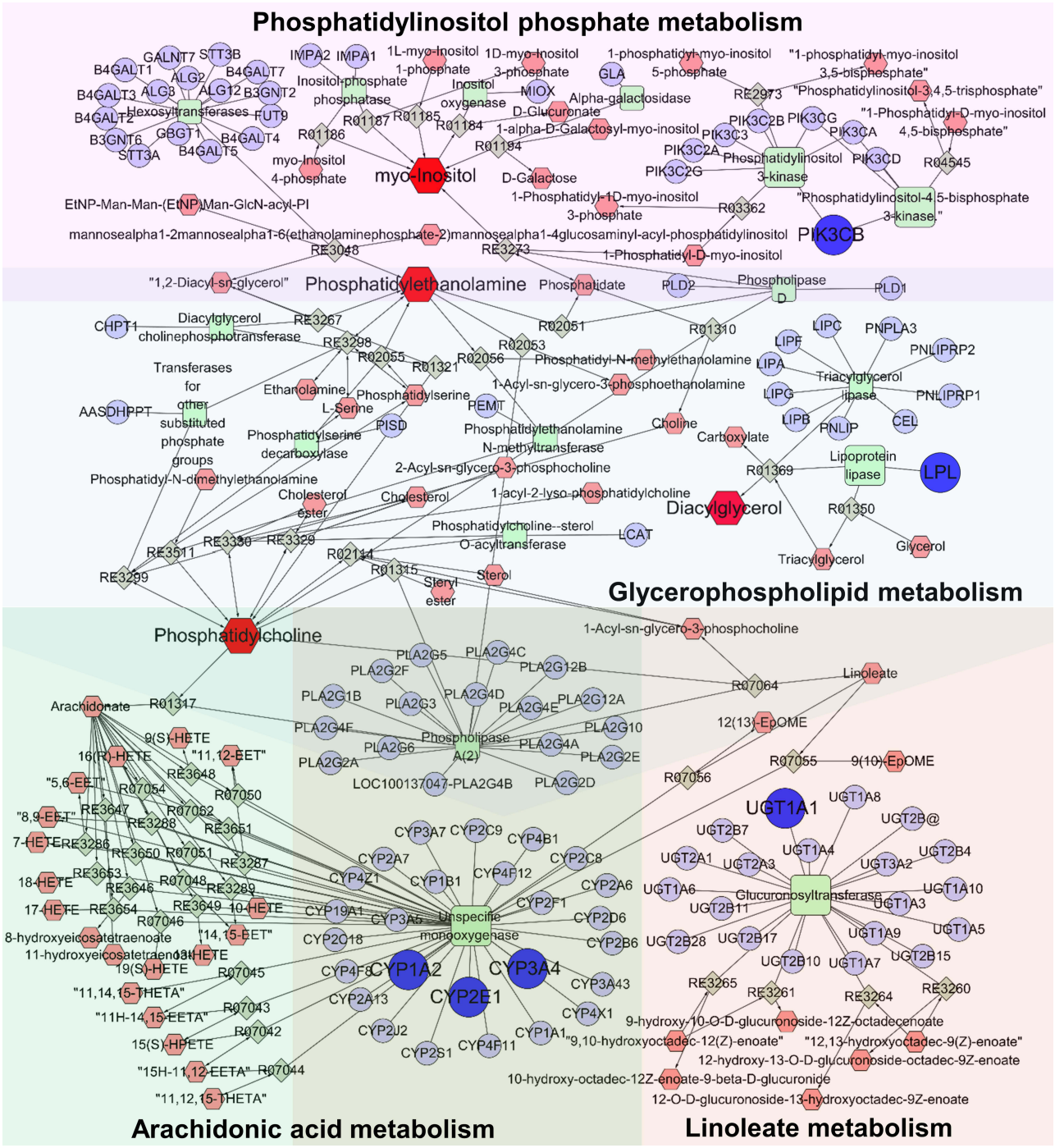

Figure 7 The compound-reaction-enzyme-gene networks of the key metabolites and targets. The red hexagons, grey diamonds, green round rectangles, and blue circles represent the active compounds, reactions, enzymes, and proteins. The key metabolites, proteins, and genes were magnified. The pathway with a purple background is Phosphatidycholinositol phosphate metabolism. The pathway with a blue background is Glycerophospholipid metabolism. The pathway with a green background is Arachidonic acid metabolism. The pathway with a yellow background is Linoleate metabolism.

Strumaroside, and Î'-Sitosterol-Î'-D-Glucoside have the lowest binding energy towards LPL (−8.4 kcal/mol) among the DS compounds (Figure 8E). These docking results demonstrate enhanced affinities between the active molecules of GDL and the primary targets, namely CYP2E1, CYP3A4, and CYP1A2.

Table 3 The Information of Key Targets, Metabolites and Pathways

NO.	Related Pathway	Key Target	Key Metabolite
1	Arachidonic acid metabolism	CYP3A4, CYP2E1, CYP1A2	Phosphatidylcholine
2	Linoleate metabolism	UGT1A1, CYP3A4, CYP2E1, CYP1A2	Phosphatidylcholine
3	Glycerophospholipid metabolism	LPL	Phosphatidylethanolamine, Phosphatidylcholine, Diacylglycerol
4	Phosphatidycholinositol phosphate metabolism	PK3CB	Phosphatidylethanolamine, myo-Inositol

Effects of GDL on the mRNA Expression Level of Key Target

We evaluated the mRNA levels of UGT1A1, CYP2E1, LPL, PIK3CB, and CYP1A2 in each group using five primers to confirm composite methodologies. Compared to the control group, the mRNA expression of UGT1A1 and PIK3CB fell intensely in the model group but increased significantly in the GDL group (Figure 8F). Compared to the control group,

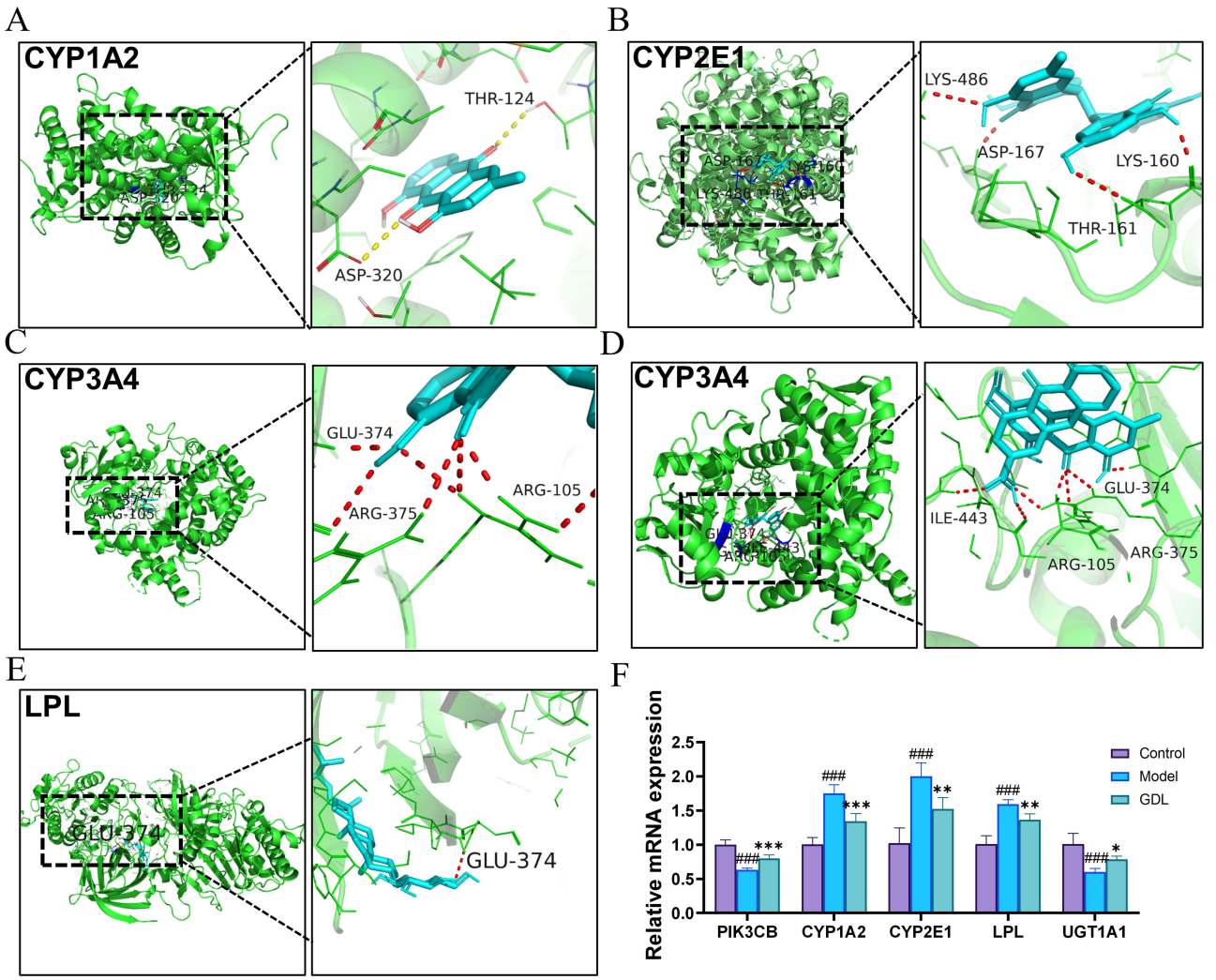

Figure 8 The 3D interaction diagrams of the active compounds of GDL and critical targets with the minimum binding energies. (**A**) The binding energy of CYP1A2 and Chrysophanol was −11.2 kcal/-mol. (**B**) The binding energy of CYP2E1 and Palmidin C was −9.6 kcal/-mol. (**C** and **D**) The binding energies of CYP3A4 towards Palmidin C and Rheidin C were −11.5 kcal/-mol. (**E**) The binding energy of LPL and Alexandrin, Daucosterol, Caproic Acid, Eleutheroside A, Sitogluside, Strumaroside, Î'-Sitosterol-Î'-D-Glucoside was −8.4 kcal/-mol. (**F**) The roles of GDL in the expression levers of UGT1A1, PIK3CB, LPL, CYP1A2 and CYP2E1. The mRNA expressions were examined by RT-PCR. β-actin was used as an internal control. Data are expressed as mean ± SEM (n = 6). $^{\#\#\#\#}p < 0.001$, compared with the control group; $^{*}p < 0.05$, $^{**}p < 0.01$, $^{***}p < 0.001$, compared with the model group.

LPL, CYP1A2, and CYP2E1 mRNA expression increased significantly in the model group but decreased significantly in the GDL group (Figure 7F). UGT1A1, CYP2E1, LPL, PIK3CB, and CYP1A2 expression levels were restored by GDL treatment.

Discussion

Previous research has identified a potential GDL therapy pathway for WD-induced neuronal damage. Dong et al revealed that GDL targets Nrf2 and NLRP3 inflammasomes in WD, which protect neural stem cells (NSCs) and increase neurogenesis in the hippocampus.[22] Zhang et al reported that the neuroprotective pathway of GDL may regulate the pink1/parkin mechanism in the hippocampus of WD-affected TX mice.[23] These findings suggest that GDL restores brain neuronal function by repairing hippocampal neurons; however, the methods are unclear. It has been demonstrated that excessively active mitophagy in the hippocampus exacerbates brain damage, as the amplification of mitophagy alters energy metabolism, resulting in the excessive consumption of mitochondria and macromolecules and accelerating neuronal death.[24,25] Therefore, we selected to examine the metabolic alterations in the hippocampus in this study. The results suggested that 28 metabolic pathways could be affected, three of which are mitochondria-related: mitochondrial Beta-Oxidation of Short Chain Saturated Fatty Acids, Medium Chain Saturated Fatty Acids and Long Chain Saturated Fatty Acids.

Metabonomics research is restricted to the characterization of possible metabolites and associated metabolic pathways but cannot delve further into their relationship. Combining network pharmacology and metabonomic findings to create a more distinct network of GDL against neuronal damage caused by WD, we can identify the material foundation, primary target, and efficacy mechanism.[26,27] We found four key mechanism pathways through the strategy. The validation results demonstrated that GDL chemical components are strongly bound to key targets. Significant changes in mRNA expression levels were observed in the key targets in the model group, while in the GDL group, they were subjected to varying degrees of recall.

GDL significantly elevated PIK3CB mRNA, which can convert phosphatidylinositol-(4,5)-bisphosphate (PIP2) into phosphatidylinositol-(3,4,5)-trisphosphate (PIP3).[28] It was reported that PIP3 could facilitate plasma membrane recruitment and activation of downstream signaling molecules, including Akt, to inhibit the FOXO signaling pathway to suppress apoptosis and autophagy.[28] This may be one of the important mechanisms by which GDL can protect WD nerve cells from death.

In contrast, the phosphorylation of a large amount of PIP2 by PIK3CB may affect other metabolic pathways, like hydrolysis. It was reported that PIP2 could also be hydrolyzed by phospholipase C (PLC) to inositol triphosphate (IP3), which mobilizes the intracellular second messengers Ca^{2+} and diacylglycerol (DG) to bind protein kinase C (PKC) to localize in an active conformation at the plasma membrane to phosphorylate diverse substrates, including phospholipase A2 (cPLA2).[29,30] Activating calcium-dependent cPLA2 makes the deacylation reaction dominant in the Lends cycle, releasing arachidonic acid (AA) and linoleic acid (LA) and damaging phospholipid components of the plasma membrane.[31,32] In the model group, phosphatidylcholine (PC), phosphatidylethanolamine (PE), phosphatidylserine (PS), phosphatidylinositol (PI), and phosphatidic acid (PA) increased DG and decreased LA. (Table 1). Model group AA metabolism did not vary significantly. The increase of DG in the model group may be related to significantly increased LPL mRNA expression levels accelerating the hydrolysis of triglycerides (TG) in triglyceride-rich lipoproteins (TRL). Then it was recruited by IP3.[33] PIP2 hydrolysis metabolism may have altered the Lends cycle balance in the model group. GDL might indirectly intervene in the hydrolysis of PIP2 through PIK3CB to repair the balance of Lends cycle, then recall PC, PE, PS, PI, and PA.

It was reported that PC, PE, PS, PI, and PA compose most of the structural phospholipids in mammalian membranes.[34] They form a phospholipid bilayer, isolate the cell contents from the environment, develop subcellular organelles, and provide a structural framework for cell activity. The fluidity, curvature and subdomain structure influence membranes related cellular processes, like bladder transport, signal transduction and molecular transport.[35] Di unsaturated PE molecular and lipids percentage with non-bilayer propensity determines the intrinsic curvature of the membrane.[36] Therefore, to keep the membrane's physical parameters within the optimal range, it is necessary to coordinate the composition of the head group and acyl chain of glycerol phospholipid, that is, the phospholipid molecular species level. Thus, model group alterations may damage biofilm. GDL recalled PC, PE, PS, PI, and PA to improve biofilm function.

The model group's LA decline may be due to free LA conversion into AA.[37] The reason for no significant changes in AA may be that it might have been metabolized by cytochrome P450 (CYP enzyme) like CYP2E1 and CYP1A2, the mRNA expression levels of which were significantly increased in the model group, to leukotriene B4 (LTB4), 5-hydroxyeicosatetraenoic acid (HETE), 12-HETE and 15-HETE, and HODE,[38,39] which caused neuroinflammation in the brain and damage nerve cells.[40,41] Thus, it is likely that AA metabolism contributes to neuroinflammation in the model group. GDL not only reduced the mRNA expression levels of CYP2E1 and CYP1A2 to prevent AA metabolism but also increased the mRNA expression levels of UDP glucuronosyltransferase family 1 member A1 (UGT1A1), which was reported to convert AA metabolites (LTB4, HETE, 12-HETE, 15-HETE, and HODE) into glucuronic acid derivatives to make them irreversibly inactivated and eliminated, to reduce inflammation.[42]

According to the outcomes of molecular docking verification, many active GDL components demonstrated a strong affinity for the four key targets in the created composite network. It had 21 active components, including all GDL-prescribed compounds. There were eight active ingredients from DH and seven active ingredients from DS. The neuroprotective impact of GDL was shown to be significantly influenced by DH and DS. In rat models of intracerebral hemorrhage (ICH), DH was also demonstrated to have brain-protective advantages by lowering hippocampus cell loss.[43] DS improves blood circulation and eliminates blood clots, and it has been utilized in China for cardiovascular and cerebrovascular illnesses for almost two hundred years.[44] In this investigation, most of DH's eight active components were anthraquinones. It has been demonstrated in prior research that anthraquinone from DH in GDL can be split into the blood in their original form and even found in the liver.[11] It has been discovered that numerous chemical components in *Salvia miltiorrhiza* can cross the blood-brain barrier and function in brain protection, including the chemical component "Tanshinone II A" analyzed by our research institute.[20] It proved that the body might transport and absorb the most active components. In particular, three targets for the anthraquinones in DH show significant binding potential and can be used to block CYP enzymes involved in AA metabolism.

GDL can activate PIK3CB to phosphorylate PIP2 to PIP3 to suppress nerve cells apoptosis and autophagy, thereby reducing IP3 and DG to regulate the balance of the Lens cycle to repair the function of biofilms at the molecular level. GDL also can inhibit the AA metabolism through CYP3A4, CYP2E1, and CYP1A2 and promote the inactivate conversion of AA metabolites through UGT1A1 to reduce inflammation. Figure 9 shows the complex mechanisms of the interaction network.

Compared to our previous study,[18] we utilized mass spectrometry, a method with great sensitivity and selectivity better suited for biological samples.[45] Our study used GC-MS and LC-MS, a complementary technique, to extract additional metabolites for a more thorough understanding of metabolic regulation.[45] We found that GDL could recall the tiny molecules of metabolites screened in the earlier stage,[18] and several phospholipid metabolic markers by the multivariate statistical data analysis. Changes in these metabolites are crucial in the early phase of programmed cell death,[46] as documented.

Conclusion

In this work, metabolomics analysis exposed that GDL recalled 29 metabolic markers. Network pharmacology uncovered important metabolic pathways and forecast GDL therapy targets and active ingredient for WD-induced neuronal injury. Combining metabolomics with network pharmacology, we located six essential targets, four critical metabolites, and four metabolic pathways. The validation of molecular docking revealed a strong affinity between GDL active compounds and key targets, indicating that Rheidin C, Palmidin C, Chrysophanol, Alexandrin, Daucosterol, Capric Acid, Eleutheroside A, Sitoglucide, Strumaroside, and Isla "- Sitoserol Isa" - D-glucoside may be the material basis of GDL. The mRNA levels of five critical targets (UGT1A1, CYP2E1, CYP2E2, PIK3CB, and LPL) were remarkably recalled by GDL. This stuty connected the metabolic phenotype with the target of action of the GDL active components to cross-validate network pharmacology and metabolomics research outcomes, enabling the discovery of more trustworthy metabolic regulatory mechanisms. This methodology may also study more traditional Chinese medications' potential pharmacological action mechanisms.

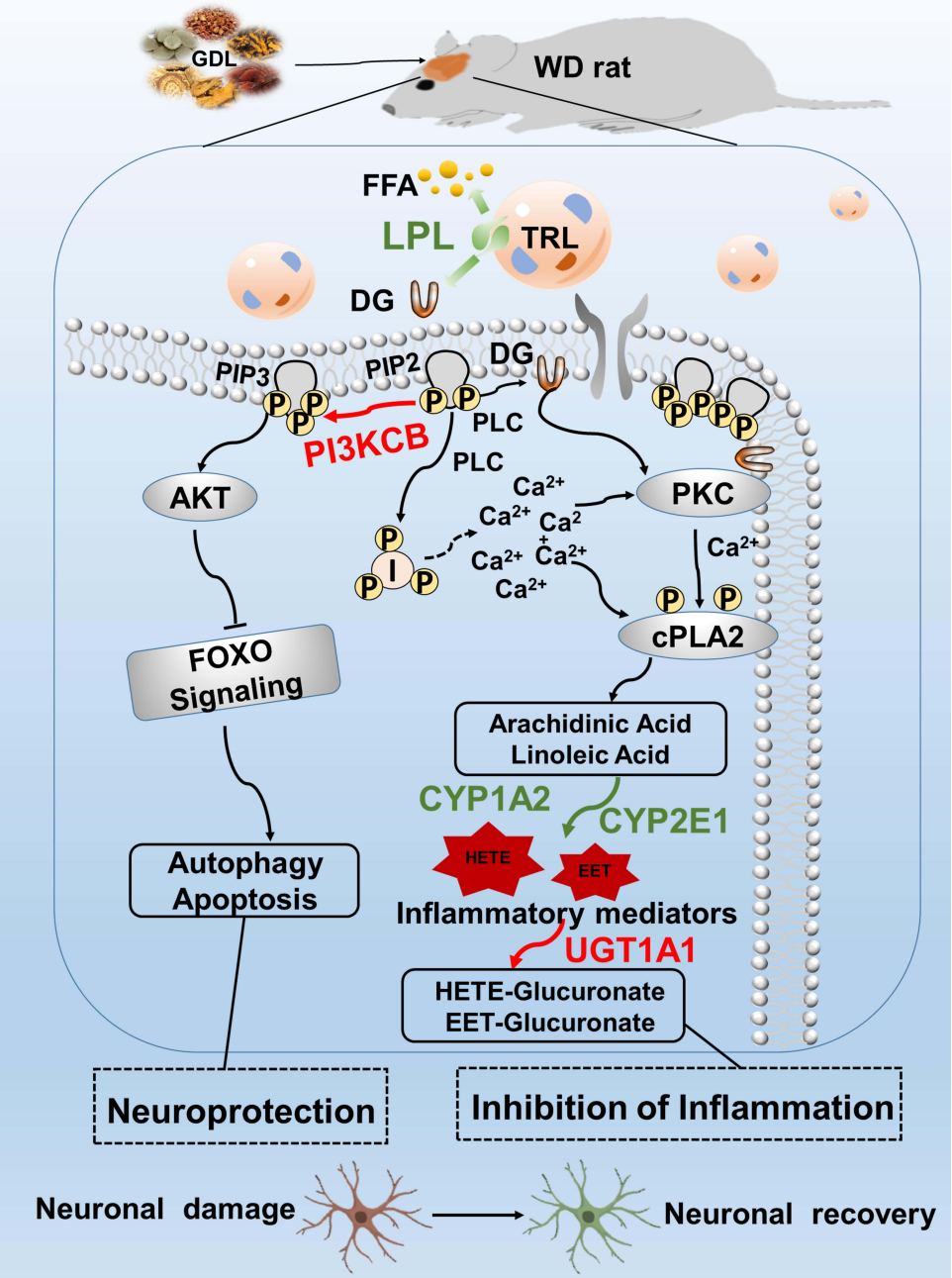

Figure 9 The mechanisms of GDL against WD-induced neuronal damage.

Funding

This study was supported by the Key Research and Development Projects of Anhui Province, China (202004j07020048).

Disclosure

The authors report no conflicts of interest in this work.

References

1. Scheiber IF, Brůha R, Dušek P. Pathogenesis of Wilson disease. *Handb Clin Neurol*. 2017;142:43–55. doi:10.1016/B978-0-444-63625-6.00005-7
2. Czlonkowska A, Gajda J, Rodo M. Effects of long-term treatment in Wilson's disease with D-penicillamine and zinc sulphate. *J Neurol*. 1996;243 (3):269–273. doi:10.1007/BF00868525

3. Kazemi K, Geramizadeh B, Nikeghbalian S, et al. Effect of D-penicillamine on liver fibrosis and inflammation in Wilson disease. *Exp Clin Transplant*. 2008;6(4):261–263.
4. Lowette KF, Desmet K, Witters P, et al. Wilson's disease: long-term follow-up of a cohort of 24 patients treated with D-penicillamine. *Eur J Gastroenterol Hepatol*. 2010;22(5):564–571. doi:10.1097/MEG.0b013e3283353df8
5. Stremmel W, Weiskirchen R. Therapeutic strategies in Wilson disease: pathophysiology and mode of action. *Ann Transl Med*. 2021;9(8):732. doi:10.21037/atm-20-3090
6. Liu S, Zhu JJ, Li JC. The interpretation of human body in traditional Chinese medicine and its influence on the characteristics of TCM theory. *Anat Rec*. 2021;304(11):2559–2565. doi:10.1002/ar.24643
7. Zhang YT, Li LH, Chen H. Research progress in the treatment of hepatolenticular degeneration with Xin'an characteristic preparation Gandouling tablets. *Chin J Exper Formulas*. 2022;28(23):97–102.
8. Lv XY. Study on the preparation technology of GDL. *J Anhui College TCM*. 1999;06:44–45.
9. Li JC, Chen MH, Huang P. Determination of berberine hydrochloride and aloe emodin in Gandouling tablets by HPLC. *J Wenshan Univ*. 2020;33 (03):33–36.
10. Chen Y, Zhang B, Cao S, et al. Gandouling combined with penicillamine improves cerebrovascular injury via PERK/eIF2α/CHOP endoplasmic reticulum stress pathway in the mouse model of Wilson's disease. *Biosci Rep*. 2018;38(5):BSR20180800. doi:10.1042/BSR20180800
11. Nian MN, Xiao L, Cui Z. Composition analysis of gandouling tablet and its metabolism in rats. *Anhui Univ Trad Chin Med*. 2022;17(1). doi:10.26922/d.cnki.ganzc.2022.000020
12. Zhang J, Xie D, Li Y, et al. Evaluation of efficacy and safety of gandouling plus sodium dimercaptosulphonate in treatment of patients with neurological Wilson's disease from China. *J TCM*. 2018;38(5):781–786.
13. Dong T, Yang WM, Wu MC, et al. Effects of gandouling on ROS and Nrf2 of neural stem cells of mice cultured in high concentration copper. *Chin J Inf TCM*. 2018;25(7):53–56.
14. Chen L, Wang S, Qin XJ, et al. Qualitative and quantitative analysis of the effective components of Coptis chinensis in Gandouling tablets by HPLC. *Chin J Inf TCM*. 2018;25(06):87–89.
15. Zhang J, Li LL, Chen HZ, et al. Clinical efficacy and safety of Gandouling plus low-dose D-penicillamine for treatment of Wilson's disease with neurological symptoms. *J Tradit Chin Med*. 2018;38(1):89–94. doi:10.1016/j.jtcm.2018.02.006
16. Johnson CH, Ivanisevic J, Siuzdak G. Metabolomics: beyond biomarkers and towards mechanisms. *Nat Rev Mol Cell Biol*. 2016;17(7):451–459. doi:10.1038/nrm.2016.25
17. Yuan H, Ma Q, Cui H, et al. How can synergism of traditional medicines benefit from network pharmacology? *Molecules*. 2017;22(7):1135. doi:10.3390/molecules22071135
18. Zhang J, Xie DJ, Bao YC, et al. 1H-NMR-based metabolomics investigation into intervention with Chinese herbs and conventional pharmaceuticals of copper-overload-induced liver injury in rats with Wilson's disease. *J Beijing Univ TCM*. 2019;42(12):1016–1023.
19. Yu XE. The protective effect of penicillamine combined with lipoic acid on mitochondrial damage of neurons in Wilson disease. *Anhui Med Univ*. 2020. doi:10.26921/d.cnki.ganyu.2020.000026
20. Zhang MY. *Study on the Cell Metabonomics and Trans Blood-Brain Barrier Transport Mechanism of Salvia Miltiorrhiza in the Prevention and Treatment of Alzheimer's Disease*. PLA Naval Medical University; 2019.
21. Geng H, Li H, Xu CC, et al. Regulatory Effect of Gandou Decoction on Wnt /β-catenin Signaling Pathway in Liver of Wilson Model Copper-loaded Rats. *Chin J Exp Tradi Med For*. 2019;25(07):75–81. doi:10.13422/j.cnki.syfjx.20190403
22. Dong T, Wu MC, Tang LL, et al. GanDouLing promotes proliferation and differentiation of neural stem cells in the mouse model of Wilson's disease. *Biosci Rep*. 2021;41(1):BSR20202717. doi:10.1042/BSR20202717
23. Zhang J, Tang LL, Li LY, et al. Gandouling Tablets Inhibit Excessive Mitophagy in Toxic Milk (TX) Model Mouse of Wilson Disease via Pink1/ Parkin Pathway. *Evid Based Complement Alternat Med*. 2020;14:3183714. doi:10.1155/2020/3183714
24. Shi R, Weng J, Zhao L, et al. Excessive autophagy contributes to neuron death in cerebral ischemia. *CNS Neurosci Ther*. 2012;18(3):250–260. doi:10.1111/j.1755-5949.2012.00295.x
25. Huang Y, Gao X, Zhou X, et al. Mitophagy in the Hippocampus is excessive activated after cardiac arrest and cardiopulmonary resuscitation. *Neurochem Res*. 2020;45(1):52. doi:10.1007/s11064-019-02916-z
26. Li T, Zhang W, Hu E, et al. Integrated metabolomics and network pharmacology to reveal the mechanisms of hydroxysafflor yellow A against acute traumatic brain injury. *Comput Struct Biotechnol J*. 2021;19:1002–1013. doi:10.1016/j.csbj.2021.01.033
27. Li S, Wang Y, Li C, et al. Study on Hepatotoxicity of Rhubarb Based on Metabolomics and Network Pharmacology. *Drug Des Devel Ther*. 2021;15:1883–1902. doi:10.2147/DDDT.S301417
28. Saravia J, Raynor JL, Chapman NM, et al. Signaling networks in immunometabolism. *Cell Res*. 2020;30(4):328–342. doi:10.1038/s41422-020-0301-1
29. Newton AC. Protein kinase C: perfectly balanced. *Crit Rev Biochem Mol Biol*. 2018;53(2):208–230. doi:10.1080/10409238.2018.1442408
30. Koundouros N, Karali E, Tripp A, et al. Metabolic fingerprinting links oncogenic PIK3CA with enhanced arachidonic acid-derived eicosanoids. *Cell*. 2020;181(7):1596–1611.e27. doi:10.1016/j.cell.2020.05.053
31. Lands WE. Metabolism of glycerolipides: a comparison of lecithin and triglyceride synthesis. *J Biol Chem*. 1958;231(2):883–888. doi:10.1016/ S0021-9258(18)70453-5
32. Hishikawa D, Hashidate T, Shimizu T, et al. Diversity and function of membrane glycerophospholipids generated by the remodeling pathway in mammalian cells. *J Lipid Res*. 2014;55(5):799–807. doi:10.1194/jlr.R046094
33. Lv Y, Wang SZ, Dai B, et al. Research progress of lipoprotein lipase in the nervous system. *Chin J Clin Pharmacol Ther*. 2022;27(09):1041–1048.
34. Van-Meer G, Voelker DR, Feigenson GW. Membrane lipids: where they are and how they behave. *Nat Rev Mol Cell Biol*. 2008;9(2):112–124. doi:10.1038/nrm2330
35. Harayama T, Riezman H. Understanding the diversity of membrane lipid composition. *Nat Rev Mol Cell Biol*. 2018;19(5):281–296. doi:10.1038/ nrm.2017.138
36. Renne MF, De-Kroon AIPM. The role of phospholipid molecular species in determining the physical properties of yeast membranes. *FEBS Lett*. 2018;592(8):1330–1345. doi:10.1002/1873-3468.12944

37. Innes JK, Calder PC. Omega-6 fatty acids and inflammation. *Prostaglandins Leukot Essent Fat Acids*. 2018;132:41–48. doi:10.1016/j.plefa.2018.03.004
38. Sonnweber T, Pizzini A, Nairz M, et al. Arachidonic Acid Metabolites in Cardiovascular and Metabolic Diseases. *Int J Mol Sci*. 2018;19(11):3285. doi:10.3390/ijms19113285
39. Gouveia-Figueira S, Martens DS, Nawrot TS, et al. Cord blood eicosanoid signatures and newborn gestational age. *Prostaglandins Other Lipid Mediat*. 2017;133:123–127. doi:10.1016/j.prostaglandins.2017.07.003
40. Stuart E, Samuel S, Jeffrey B, et al. Arachidonic acid closes innexin/pannexin channels and thereby inhibits microglia cell movement to a nerve injury. *Sci Direct*. 2013;73(8):621–631. doi:10.1002/dneu.22088
41. Gian LR. Dietary n-6 and n-3 polyunsaturated fatty acids: from biochemistry to clinical implications in cardiovascular prevention. *Biochem Pharmacol*. 2009;77(6):937–946. doi:10.1016/j.bcp.2008.10.020
42. Turgeon D, Chouinard S, Belanger P, et al. Glucuronidation of arachidonic and linoleic acid metabolites by human UDP-glucuronosyltransferases. *J Lipid Res*. 2003;44(6):1182–1191. doi:10.1194/jlr.M300010-JLR200
43. Wang K, Hu CJ, Zhao X, et al. Based on the brain protective effects of raw rhubarb and wine rhubarb on ICH rats, the theory of "wine production and lifting" was discussed. *Chin J Exper Formulas*. 2019;25(06):130–135. doi:10.13422/j.cnki.syfjx.20182405
44. Ma XJ, Yang J, Ma GR, et al. Research progress on modernization of traditional Chinese medicine Salvia miltiorrhiza. *Chin J TCM*. 2022;47(19):5131–5139. doi:10.19540/j.cnki.cjcmm.20220808.101
45. Li MY, Lin XC, Zhao MM. Advantages and disadvantages of nuclear magnetic resonance spectroscopy and mass spectrometry in metabolomics. *J Guilin Univ Electr Sci Technol*. 2022;42(04):311–317. doi:10.16725/j.cnki.cn45-1351/tn.2022.04.008
46. Maiese K. FoxO proteins in the nervous system. *Anal Cell Pathol*. 2015;569392. doi:10.1155/2015/569392